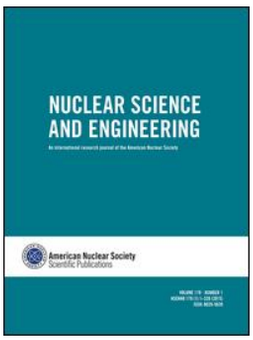

Nuclear Science and Engineering

ISSN: (Print) (Online) Journal homepage: https://www.tandfonline.com/loi/unse20

Compensated Feed water Pump Control Analysis of Effect of Base-Load Electricity Demand Reduction on Nuclear Steam Supply System

Frederick Agyemang, Stephen Yamoah & Seth Kofi Debrah

To cite this article: Frederick Agyemang, Stephen Yamoah & Seth Kofi Debrah (2022): Compensated Feed water Pump Control Analysis of Effect of Base-Load Electricity Demand Reduction on Nuclear Steam Supply System, Nuclear Science and Engineering, DOI: 10.1080/00295639.2022.2132102

To link to this article: https://doi.org/10.1080/00295639.2022.2132102

Published online: 05 Dec 2022.

NUCLEAR SCIENCE AND ENGINEERING

DOI: https://doi.org/10.1080/00295639.2022.2132102

Compensated Feed water Pump Control Analysis of Effect of Base-Load Electricity Demand Reduction on Nuclear Steam Supply System

Frederick Agyemang,[a]* Stephen Yamoah,[a,b] and Seth Kofi Debrah[a,b]

[a]*University of Ghana, Graduate School of Nuclear and Allied Science, P.O. Box LG 80, Legon, Accra, Ghana*
[b]*Nuclear Power Institute, Ghana Atomic Energy Commission, P.O. Box LG 80, Legon, Accra, Ghana*

Received February 14, 2022
Accepted for Publication September 30, 2022

Abstract — *The effect of compensated feedwater (FW) pump control on a nuclear steam supply system with a significant reduction of baseload electricity demand as a common-cause failure could result in temperature elevation of the reactor coolant system and corresponding pressure increases in the pressurizer and steam generators above the set points. The shutting and opening of the pressure relief valve causes the fluid flow rate to transition from laminar to turbulence flow, where a sudden burst, chaotic movement, and inertial forces and weight of the fluid have the potential to cause a break in pipelines leading to a loss-of-coolant accident. This study employs the Fourier transform to simulate the impact of force as the power spectral density (in dBm/Hz) measured in 1 to 99 label harmonics over a specified time window using MATLAB/Simulink library tools. The experimental results show that compensated FW pump control could significantly reduce the effect of turbulence and reveal a perturbation settlement state prior to steady-state laminar flow.*

Keywords — *Nuclear steam supply system, FW pump control, water hammer, power spectral density, compensated drive control.*

Note — *Some figures may be in color only in the electronic version.*

I. INTRODUCTION

A significant reduction of baseload electricity demand for domestic and industrial applications may cause the temperature of the reactor coolant system (RCS) to increase as well as corresponding pressure increases in the pressurizer and steam generators (SGs). The short fall in terms of electricity demand triggers the integrated plant control system of the nuclear steam supply system (NSSS) instrumentation and control (I&C) into action. Feedwater (FW) pump control involves the fluid flow and control signal (information flow). The two manipulated variables involved are (1) motor speed control and (2) the safety and pressure control valve since the amount of heat release from the nuclear chain reaction must be proportional to the amount of heat taken away for the production of electrical energy.

The main FW pump control system[1] takes suction from the condenser (reservoir) and transfers water through a pressure relief valve and a network of pipelines to the SG. The process involves shutting and opening the

*E-mail: fagyemang007@st.ug.edu.gh

pressure relief valve, which causes the fluid flow rate to transition from laminar to turbulence flow as water hammer, a phenomenon in the water supply piping system.[2,3]

The dynamic changes in the mass flow rate, the pressure changes of the inflow fluid into the SG, the kinetic energy of the fluid, and the dynamic friction,[4] with loading on pipes,[5] particularly the high-pressure pipes in the nuclear application,[6] result in water hammer. In longer pipes, the effect of valve shut or open for a few milliseconds triggers water hammer.[7] The analysis of turbulence flow is very complex, and the parameters that affect the flow regime depend on the Reynolds number.[8]

A break or leakage could result in elevated temperatures in the RCS of the primary cooling system.[9] Reduction of coolant flow or total loss of cooling is a recipe for a loss-of-coolant accident (LOCA) in the nuclear power plant[10] (NPP). The follow-up condition could ignite core spraying,[11] leading to emergency shutdown of the nuclear reactor. A blowdown period of 0 to 30s due to a large break in the primary circuit must be expelled rapidly to avoid a worst-case scenario, a period that occurs between 30 and 40s following the start of LOCA (Ref. 12). The injection of the emergency core cooling system into action for a small break is determined by the interplay between the core power level, axial power shape, break size, high head safety, and the pressure at which injection begins. For the Westinghouse pressurized water reactor (PWR), a typical break should be between 2 to 4 in. (5.08 to 10.16 cm) (Ref. 1).

Earlier investigation of steam condensation induced water hammer (CIWH), performed in the PMK-2 facility of the full-pressure thermohydraulic model on NPP (Ref. 13), concluded that a water hammer pressure peak at a specific pressure range, where the steam bubble is shown to be "only formed" and shows a "nervous" shiver motion, is a challenge that should be addressed.

Another investigation of the steam CIWH phenomenon of full-pressure thermodynamics of the VVER-440/312 type of NPP of a scaled-down model, where the experimental and theoretical modes of the dynamics of the pressure wave propagation of the vapor void fraction along the pipeline "steam bubble collapse," confirms the six conditions of Griffith of screening of the steam/water piping system.[14,15]

An experimental and theoretical investigation was conducted on multiple events of condensation of induced water hammer of the VVER-440/312 thermal-hydraulic model of the NPP, where the effect of the thermal-hydraulic model of water hammer on a fully powered NPP located in Atomic Energy Research Institute, Budapest, Hungary, was studied. A similar investigation was also conducted in the Rig of Safety Assessment (ROSA) facility in Japan on two-phase flow.[16] The investigations concluded, "full time numerical simulation of the ROSA could not be carried out"; however, the investigations provided a clearer insight into the happenings of the physical phenomena. Investigation in nuclear application is vital for the purposes of safety and the likelihood of a major break in the piping network leading to LOCA (Ref. 16).

The steam CIWH phenomenon experiment of the VVER-440/312 NPP provided a planned large database of upper and lower flooding mass flow rates of different pipe geometries.[17] The WAHA3 code describes supersonic two-phase flow transients in pipelines, while further studies are required in other physical parameters, part of which this study seeks to analyze.

II. THEORIES

In fluid dynamics,[18] the total pressure in NSSS of the thermal liquid domain of the piping network connected to the SG is equal to the static pressure plus the system dynamic. This principle forms the basis of Bernoulli's equation in fluid dynamics, mathematically expressed as

$$\frac{dm}{dt} = \dot{m}_{in} + \dot{m}_{out} \ , \tag{1}$$

where $\dot{m}_{in}$ and $\dot{m}_{out}$ are the mass flow in and mass flow out of the piping network.

In nuclear application, the accumulation of fluid in SG is expressed as

$$Acc = In - Out + Gen - Con. \tag{2}$$

The principles obey the laws of conservation of mass and energy, where the balance accumulation is equal to the intake minus the outlet plus generation minus consumption.

The FW pump is driven by an electrical motor, and the positive threshold speed of the motor shaft is

$$\omega = \begin{cases} \omega_{Th,} & \omega_{In}\epsilon < 0 \\ (1-\lambda)\omega_{Th} + \lambda|\omega_{In}|, & \omega_{In}\epsilon < \omega_{Th} \\ |\omega_{In}|, & \omega_{In}\epsilon \geq \omega_{Th} \end{cases} , \tag{3}$$

where

ω = shaft speed

Th = threshold values

In = input value

ϵ = mechanical orientation of the pump

(+1), (−1) = positive and negative, respectively.

The term λ determines the width of the transition region and is defined as

$$\lambda = 3\left(\frac{\omega_{In}}{\omega_{Th\epsilon}}\right)^2 - 2\left(\frac{\omega_{In}}{\omega_{Th\epsilon}}\right)^3. \tag{4}$$

The characteristics of the pump parameterization are determined by two variables: the head of the pump (orifice) and the capacity in terms of volumetric flow rate. The conversion between the pump head and the pressure is expressed as

$$\Delta H = \frac{\Delta P}{\rho g}, \tag{5}$$

where

ΔH = pump head

ΔP = static pressure

ρ, g = density and acceleration due to gravity, respectively.

The conversion of the flow capacity and that of the mass flow rate is given by

$$Q = \frac{\dot{m}}{\rho}, \tag{6}$$

where Q is the flow capacity of the pump and $\dot{m}$ is the mass flow rate.

The flow capacity of the pump is determined by

$$\frac{Q_R}{Q} = \frac{\omega_R}{\omega}, \tag{7}$$

where the subscript R is the reference value.

The impact of the pump rotational speed change is governed by the affinity law, and the flow capacity is determined by

$$\frac{Q_R}{Q} = \frac{\omega_R}{\rho}, \tag{8}$$

where ω is the saturated shaft speed and R is the reference value. Hence, Q_R is expressed as

$$Q_R = \frac{\omega_R}{\omega}\frac{\dot{m}}{\rho}. \tag{9}$$

In a lookup table, the value of flow capacity employs the reference pump head and brake power.

The flow capacity is also determined by

$$\frac{Q_R}{Q} = \frac{\omega_R}{\omega}. \tag{10}$$

The pressure rise of the pump head is determined by

$$\frac{\Delta H_R}{\Delta H} = \frac{\omega_R^2}{\omega^2}. \tag{11}$$

Affinity laws are employed in relation to the pump capacity, head, and power, where one-dimensional (1-D) parameterization of the reference pump is

$$\Delta H_R = \Delta H(Q_R)\ . \tag{12}$$

And, two-dimensional (2-D) parameterization is the flow capacity and shaft speed:

$$\Delta H_R = \Delta H(Q, \omega)\ . \tag{13}$$

The expression of ΔH during pressure rise is

$$\Delta P = \frac{\omega^2}{\omega_R^2}\rho g \Delta H_R\ . \tag{14}$$

The reduction in shaft speed of 2-D parameterization is

$$\Delta P = \rho g \Delta H_R\ . \tag{15}$$

The torque of the shaft is determined by

$$\frac{P_R}{P} = \frac{\omega_R^3 \rho_R}{\omega^2 \rho}, \tag{16}$$

where P_R is the reference brake power and P is the brake power in 1-D parameterization:

$$P_R = P(Q_R)\ . \tag{17}$$

The 2-D parameterization of the instantaneous shaft speed and flow capacity is

$$P_R = P(Q, \omega)\ . \tag{18}$$

The shaft torque and the brake power are expressed as

$$P = T\omega\,, \tag{19}$$

where T is the torque. The instantaneous shaft torque is given as

$$T = \frac{\omega^2}{\omega_R^3}\frac{\rho}{\rho_R}P_R\ . \tag{20}$$

The reduced shaft speed ratio in 2-D parameterization is

$$T = \frac{1}{\omega_R}\frac{\rho}{\rho_R}P_R. \tag{21}$$

The rotational dynamics of the centrifugal pump generate pressure rise at the outlet of the pump (pumps differ in their characteristics).

The pressure relief valve is the second variable parameter of the study in addition to the FW pump. The equation for the valve is given as

$$q\ = C_v f(l)\sqrt{\frac{\Delta P_v}{g_s}}, \tag{22}$$

where the flow rate q, through the value is equal to a constant C_v, which is the coefficient of the valve, the lift function $f(l)$ times the square root of ΔP_v across the value dividing specific gravity g_s. The valve has installed and noninstalled characteristics.

The mass balance of the flow rate of the inlet port A and outlet port B of the valve is given as

$$O = \dot{m}_A + \dot{m}_B\ . \tag{23}$$

The momentum of the differential pressure is given as

$$\Delta p = \frac{1}{2\rho}\left(1 - \frac{S_R^2}{S^2}\right)v_R\sqrt{v_R^2 + v_{Rc}^2}\,, \tag{24}$$

where the fluid velocity restriction v_R and the critical velocity restriction v_{RC} are given as

$$v_R = \frac{\dot{m}_A}{C_d\rho S_R}$$

and

$$v_{Rc} = \frac{\mathrm{Re}_c\mu}{C_d\rho S_R}\sqrt{\frac{\pi}{4S_R}}, \tag{25}$$

where

Δp = pressure differential

ρ = liquid density

μ = liquid dynamic viscosity

S = cross-sectional area at ports A and B

S_R = cross-sectional area of pump restriction

v_R = fluid velocity restriction

v_{Rc} = critical velocity restriction

Re_c = critical Reynolds number

C_d = discharge coefficient.

When the compensated pressure recovery is *Off*,

$$P_A - P_B = \Delta P\,, \tag{26}$$

where P_A is the pressure at port A and P_B is the pressure at port B.

When the compensated pressure recovery was turned *On*,

$$P_A - P_B = \Delta P\frac{\sqrt{1 - \left(\frac{S_R}{S}\right)^2\left(1 - C_d^2\right)} - C_d\frac{S_R}{S}}{\sqrt{1 - \left(\frac{S_R}{S}\right)^2\left(1 - C_d^2\right)} + C_d\frac{S_R}{S}}. \tag{27}$$

With compensated pressure recovery, the slowdown of fluid velocity increases the pressure locally, accompanied by an increase in turbulence flow with thermal heat friction in the fluid.

III. RESULTS AND DISCUSSION

The network loop consists of the condenser, FW pump, FW pump controller, pressure control valve, SG level controller, SG, steam sensors S_1 and S_3, and fluid sensors S_2 and S_4 (Fig. 1). The sensors fulfill the system requirements of verification and validation,[19] of integration of existing analogue technology and digital technology of the nuclear I&C system.

The equations and the modules used for the analysis employed MATLAB/Simulink library tools. The condensation of steam forms the pool of water as a condenser (reservoir) that serves as the infinite supply of fluid to the SG (Fig. 2). The experiment model provided FW pump control without a compensator and the second model with a compensator.

The flow rate and pressure signals were monitored on an oscilloscope while the perturbation response was monitored on a spectrum analyzer, where the response depicted the actual behavioral activities (turbulent activities) of the fluid

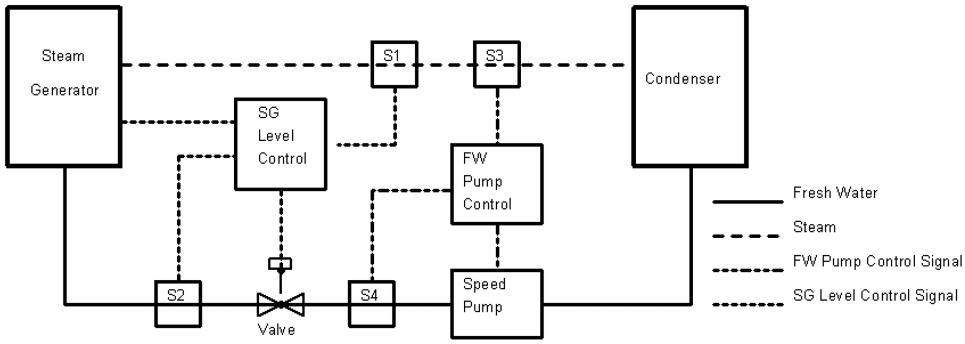

Fig. 1. Block diagram of FW pump control.

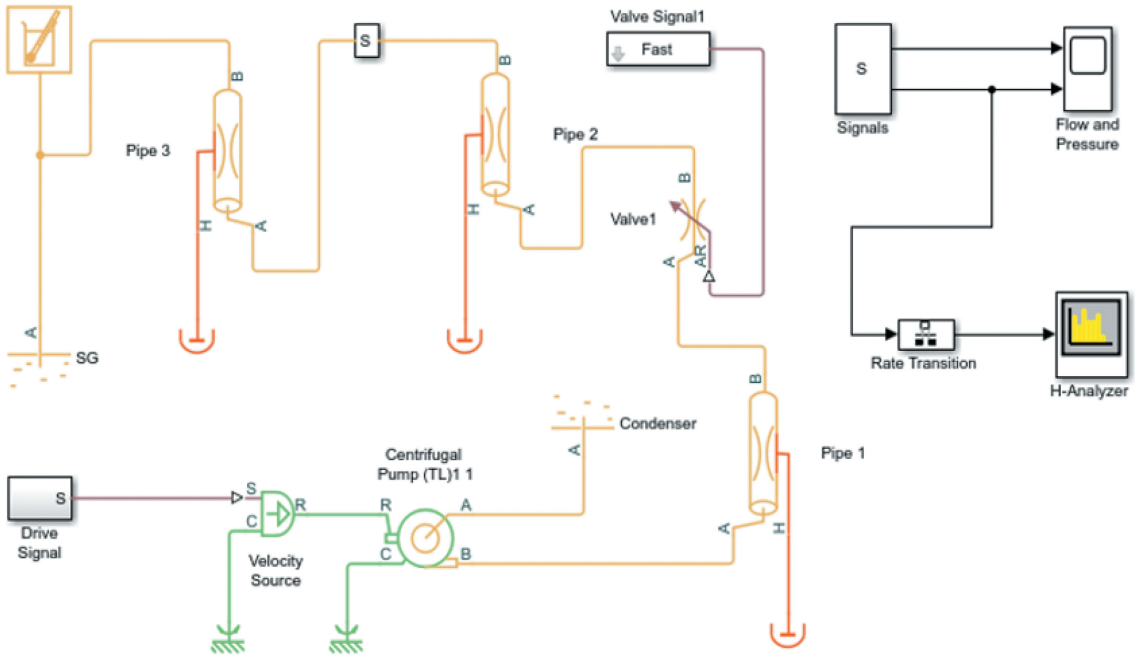

Fig. 2. Pressure recovery compensated FW pump control.

within the pipes without a compensator (Fig. 3). Other simulations carried out used a different compensated drive control signal.

For a typical PWR SG, the design pressure is 172 bars, and the operating pressure is 155 bars. The full load pressure is between 63 to 69 bars depending on the number of plant loops. The plot of Fig. 3 shows the pressure of 1 bar (for the purposes of simulation). The waveform is complex to analyze due to the nature of the components involved. The cumulative effects of perturbation of both the positive and the negative sides of the waveform have a stronger impact on the piping and its fittings.

Other inputs applied included sine wave to observe the effect of lead or lag compensation, which had no significant effect on compensation due to the presence of noise perturbations. In addition, a pump speed input signal was applied, as well as an input step response (Fig. 4). The use of a variety of signal sources was for the generation of the desired velocity variation profile.

After a series of comparisons and simulations, with the difference between the random numbers and the band-limited white noise of perturbations of the randomly distributed waveform, the observation produced an output at a specific sampling rate related to correlation of the noise. The introduction of band-limited white noise as an input signal compensator provided randomly distributed numbers suitable in continuous and hybrid systems (Fig. 5).

The velocity source was employed as an ideal angular velocity to generate differential velocity proportional to the physical input signal. The mechanical rotation of physical ports *R* and *C* drive the applied source, such that

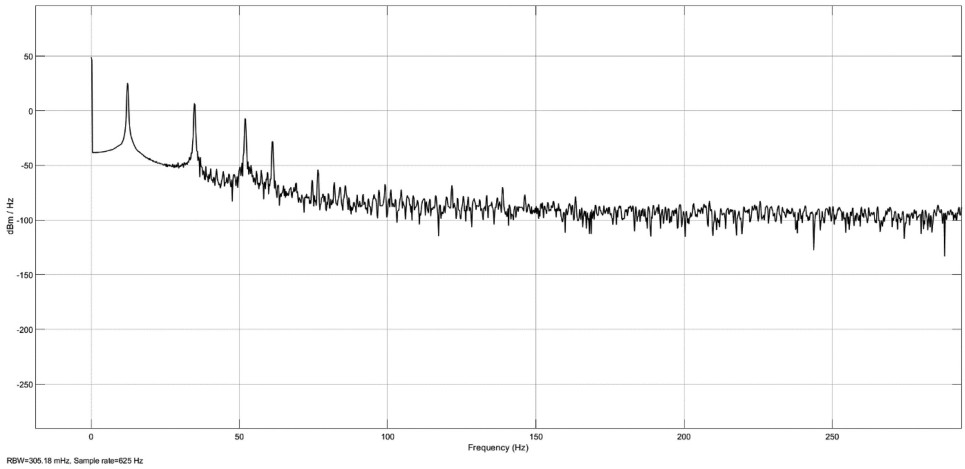

Fig. 3. Effect of turbulence without compensator.

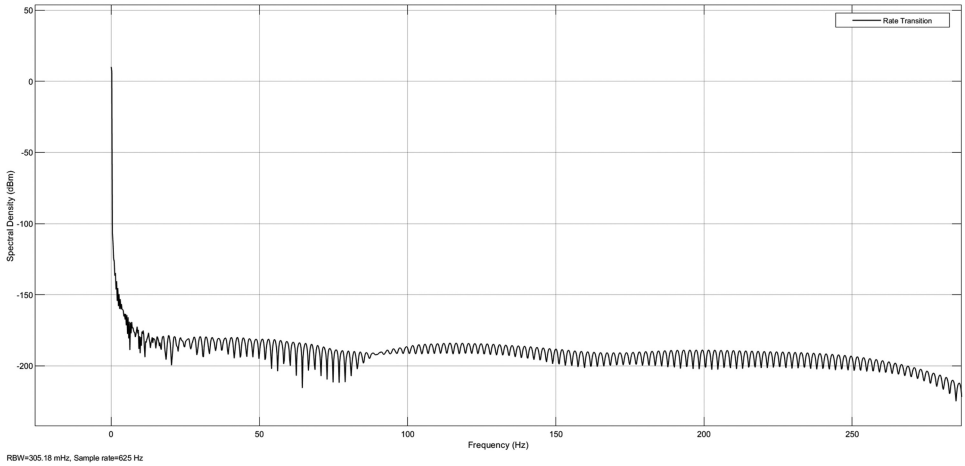

Fig. 4. Pump speed as input signal source.

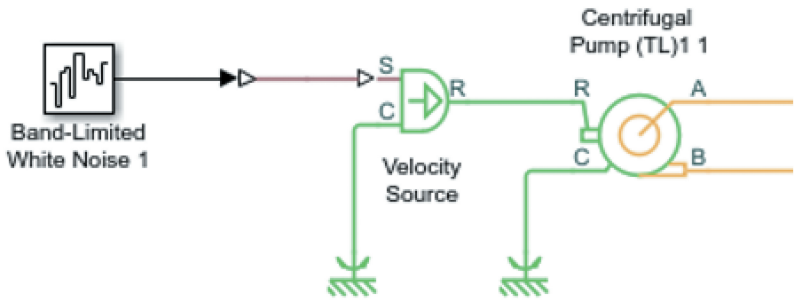

Fig. 5. Compensated band-limited white noise input signal.

the relative velocity w can be determined as $w = w_R - w_C$, where w_R and w_C are the angular velocities of R and C.

The effect of hammering shown as a periodogram is due to the pump head and the turbulence of water within the confined walls of the transporting pipes forming the thermal fluid network. The sequence of correlation time of the noise has the sampling frequency rate of 625 Hz with resolution bandwidth as high as 305.18 mHz (Fig. 6). In theory, continuous white noise has a correlation time of zero, with a flat power spectral density (PSD) of the total energy.

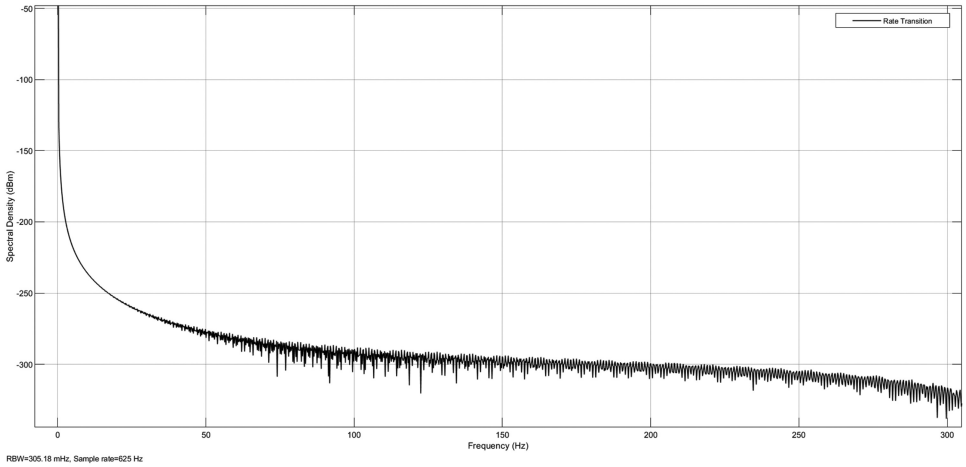

Fig. 6. Effect of water hammering.

The simulation results illustrate the effect of the white noise random sequence with correlation time being smaller than the shortest time constant of the system. The dynamics of the system operation is much faster, with *fmax* representing the bandwidth of the system in rads per second (Fig. 7). The value of a constant (*mdot0*) as the Reynolds number (ratio of inertial forces and viscous forces) is above unity, which was 5.003; any increment in the constant has no significant effect in the correlation sequence.

The relative mass flow perturbation and relative pressure perturbation is −1, where the mass flow perturbation is zero, after reaching the set point. With a negative Reynolds value, the hammering effect was reduced, suggesting that the compensated pressure control in the FW pump control system was efficient.

The introduction of an input source signal to the velocity source of the FW pump control I&C system to serve as a countereffect of the eddy's high oscillation is to neutralize chaotic turbulence that could lead to LOCA.

III.A. Analysis of PSD

The perturbations of the randomly distributed signal analyzed were to determine the PSD of the power present in the signal as a function of frequency due to the water hammer effect. The shape of the frequency spectrum as a functional variation of the amplitude spectral density is proportional to the variation of the signal voltage level. The energy concentration was calculated within a finite time interval by the integration of $x^2(t)$ using Parseval's theorem, while in accordance with Fourier analysis, the physical signals decomposed into a number of discrete frequencies.

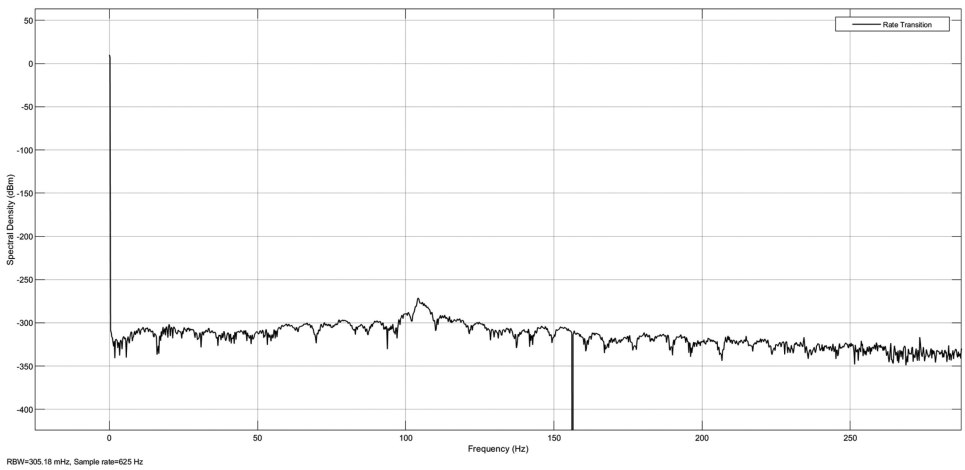

Fig. 7. Perturbations randomly distributed.

The energy E according to Parsevel's theorem is[20]

$$E = \int_{-\infty}^{\infty} |x(t)|^2 dt \ . \tag{28}$$

The Fourier transform $x(t)$ of frequency $f(Hz)$ with energy spectral density is defined as

$$\overline{S}_{xx}(f) = |\widehat{x}(f)|^2 \, , \tag{29}$$

where the function $\overline{S}_{xx}$ is the autocorrelation of $x(t)$, a complex random process of the Fourier transform,[21] and the density function contained in the signal is $|\widehat{x}(f)|^2$.

The turbulence in pipelines over a given frequency band is calculated based on the average power density in the perturbation over a particular frequency band. For a single time series, the estimated PSD over a specified time window is $-N \leq n \leq N$. The PSD for a discrete time variable $x_n = x\ (n\Delta t)$ for a total measurement period $T = (2N + 1)\ \Delta t$ is given as

$$S_{xx}(f) = \lim_{N\to\infty} \frac{(\Delta t)^2}{T} \left| \sum_{n=-N}^{N} x_n e^{-i2\pi f n \Delta t} \right|^2 . \tag{30}$$

The total power of the signal is contained in the one-sided PSD of the frequency interval from the direct-current (DC) component to half of the Nyquist rate. The signal consists of frequency f, and additional noise N, at a sampling frequency with the signal length in the samples. The default setting requiring a random number generator is

$$S_{xx}(f) = \lim_{N\to\infty} \frac{(\Delta t)^2}{T} |\widehat{x}(f)|^2 \, , \tag{31}$$

where $S_{xx}(f)$ is the power spectrum of the time series $x(t)$.

The distortion measurement of harmonics is measured based on frequency (in Hz) and PSD (in dBm), where dBm or dB_{mW} (decibel-milliwatts) is the power level expressed in decibels with reference to 1-mW experience as in every impact of water hammer, where the distortions are measured in 1 to 99 label harmonics as shown in Fig. 8. The power spectral $Sxx(f)$ of the water hammer in a time series $x(f)$ describes the distribution of power into frequency components composed of the turbulent effect due to eddies into a number of discrete spectral frequencies over a continuous range.

The summation for the period of 1 to 99 in Table I of the tabulated PSD, with the delta provided for the frequency range of 1.01725 to 103.963 Hz and the total PSD of −2488.47 dBm.

The total value of −2.48847 decibel is the single estimated PSD obtained from a finite number of samplings. Any harmonics that are outside the frequency span of the spectrum analyzer are not included and labeled as (-)*Inf* in the tabulated data. The PSD is achieved when the additional noise N (and thus T) approaches infinity and the expected value is formally applied.

The total power of the signal is contained in one-sided PSD of the frequency interval from the DC component to half

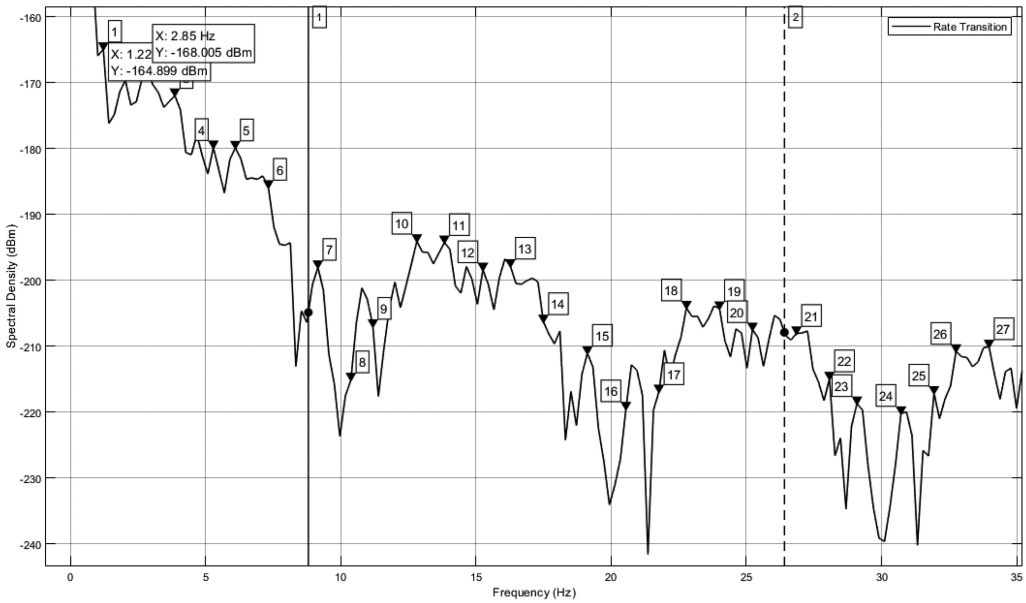

Fig. 8. PSD of specific window.

of the Nyquist rate, where the signal consists of frequency f and additional noise N at a sampling frequency with the signal length in the samples. The default setting requires a random number generator.

The highest-order term reaches

$$A_0 = S_{xx}(f) \ . \tag{32}$$

However, the unknown values are $\varepsilon^1 A_1$ and $\varepsilon^2 A_2$:

$$A = S_{xx}(f) + \varepsilon^1 S_{xx}(f)_1 + \varepsilon^2 S_{xx}(f)_2 + \dots \ , \tag{33}$$

where

$$A = A_0 + \varepsilon A_1 + \varepsilon^2(0) \tag{34}$$

and

$$\varepsilon^2(0) = A_{pss} = 0_a \ , \tag{35}$$

where A_{pss} is the perturbation settlement state (PSS) and is equal to quasi steady state 0_a:

$$\begin{aligned} A = & \lim_{N\to\infty} \frac{(\Delta t)^2}{T} \left| \sum_{n=-N}^{N} x_n e^{-i2\pi f n \Delta t} \right|^2 \\ & + \varepsilon^1 \lim_{N\to\infty} \frac{(\Delta t)^2}{T} \left| \sum_{n=-N}^{N} x_n e^{-i2\pi f n \Delta t} \right|^2_1 \\ & + \varepsilon^2 A \lim_{N\to\infty} \frac{(\Delta t)^2}{T} \left| \sum_{n=-N}^{N} x_n e^{-i2\pi f n \Delta t} \right|^2_{pss} . \end{aligned} \tag{36}$$

TABLE I

Estimated PSD

Number	Frequency (Hz)	Power (dBm)	Number	Frequency (Hz)	Power (dBm)	Number	Frequency (Hz)	Power (dBm)
1	1.01725	−143.06	34	35.4004	−24.83	67	70.5973	−39.01
2	2.03451	−3.28	35	36.8245	−21.97	68	71.4111	−39.49
3	2.84831	−0.05	36	37.6383	−26.52	69	72.6219	−30.08
4	4.06901	−2.87	37	39.0625	−32.92	70	73.6491	−27.43
5	5.28971	−7.09	38	40.0798	−39.24	71	74.6663	−28.13
6	6.10352	−5.26	39	40.8936	−30.02	72	72.2767	−28.68
7	7.12077	−8.04	40	41.9108	−29.89	73	76.4974	−29.65
8	8.13802	−16.24	41	42.9281	−21.7	74	77.5146	−40.13
9	9.15527	−19.85	42	43.9453	−19.35	75	78.5319	−37.93
10	10.7829	−21.32	43	45.3695	−22.74	76	79.9561	−41.11
11	11.8001	−23.25	44	46.1833	−20.43	77	80.9733	−34.34
12	12.8174	−13.17	45	47.2005	−20.47	78	81.9906	−30.78
13	13.8346	−12.21	46	48.0143	(-)*Inf*	79	83.0078	−27.98
14	14.8519	−16.04	47	49.235	−30.41	80	84.0251	−26.49
15	15.8691	−16.46	48	50.6592	−33.15	81	85.0423	−21.97
16	17.0898	−15.33	49	51.473	−28.83	82	86.0596	−24.98
17	17.9036	−21.32	50	52.6937	−19.79	83	86.8734	−28.41
18	19.1243	−25.43	51	53.7109	−16.97	84	87.8906	−28
19	19.7347	(-)*Inf*	52	54.7282	−18.1	85	89.1113	−31.73
20	20.752	−28.18	53	55.3385	−16.81	86	90.332	−37.14
21	21.9727	−25.48	54	56.9661	−14.85	87	91.3493	−35.93
22	22.9899	−18.57	55	57.5765	−16.86	88	92.3665	−34.56
23	24.0072	−16.96	56	59.0007	−16.13	89	93.5872	−31.56
24	25.2279	−20.69	57	60.0179	−4.84	90	94.6045	−33.52
25	26.0417	−17.95	58	60.8319	−12.08	91	95.8252	−31.58
26	27.0589	−19.1	59	61.6455	−21.05	92	96.8424	−30.75
27	28.0762	−23.96	60	62.8662	−13.46	93	97.8597	−32.75
28	29.0934	−28.19	61	63.8835	−15.73	94	98.877	−33.48
29	30.721	−32.63	62	65.3076	−19.81	95	99.6908	−38.64
30	31.5248	−29.63	63	66.1214	−18.51	96	100.911	−38.36
31	32.7555	−20.3	64	67.1387	−21.52	97	101.522	−37.91
32	33.7728	−19.71	65	68.3594	−33.46	98	102.743	−32.58
33	34.79	−25.17	66	69.1732	−32.08	99	103.963	−32.08

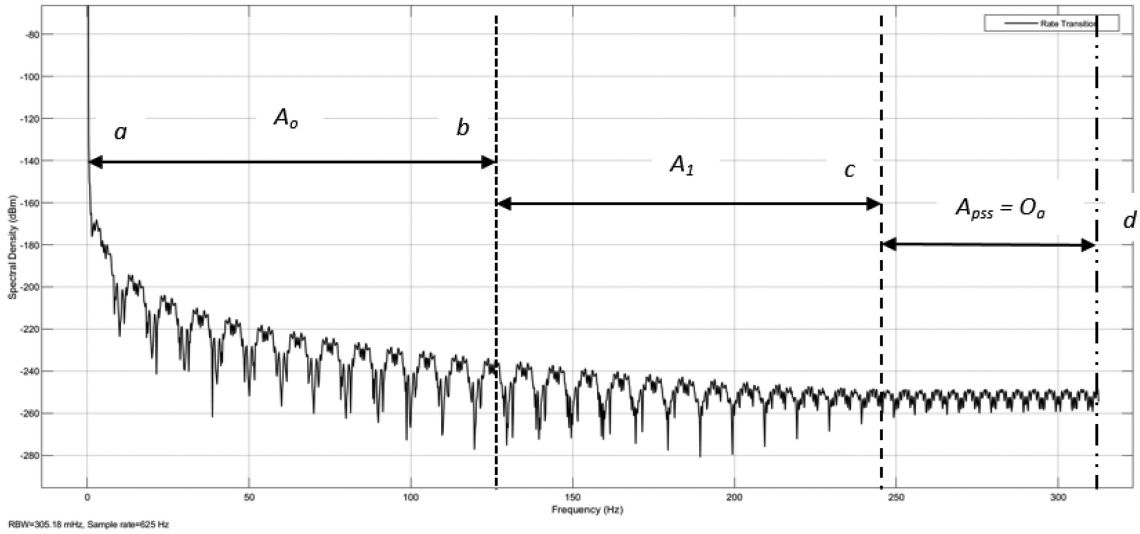

Fig. 9. Perturbation settlement state.

The simulation illustrates the distortion measurement from the spectrum analyzer that displays the harmonics distortion and intermodulation distortion measurement of the perturbation state (Fig. 9).

The PSS is a state where turbulence seems to have settled into a quasi state as the signal follows a regular pattern. From perturbation theory, the approximate solution has a power series of a small parameter ε.

With one-half of the frequency spectrum, the more positive the figure of the PSD (in dBm/Hz) is, the more the effect of the water hammer on the piping system is (Fig. 10).

The mathematical formula of the perturbation expressed as PSD (in dBM/Hz) of one-half of the frequency spectrum indicates that the more negative the cumulative sum is, the lesser the effect of the water hammer is. Additionally, a state where turbulence seems to have settled, otherwise known as PSS, where a second unknown parameter is to be known as the quasi perturbation state, indicates a repeated pattern of the quasi-settlement state.

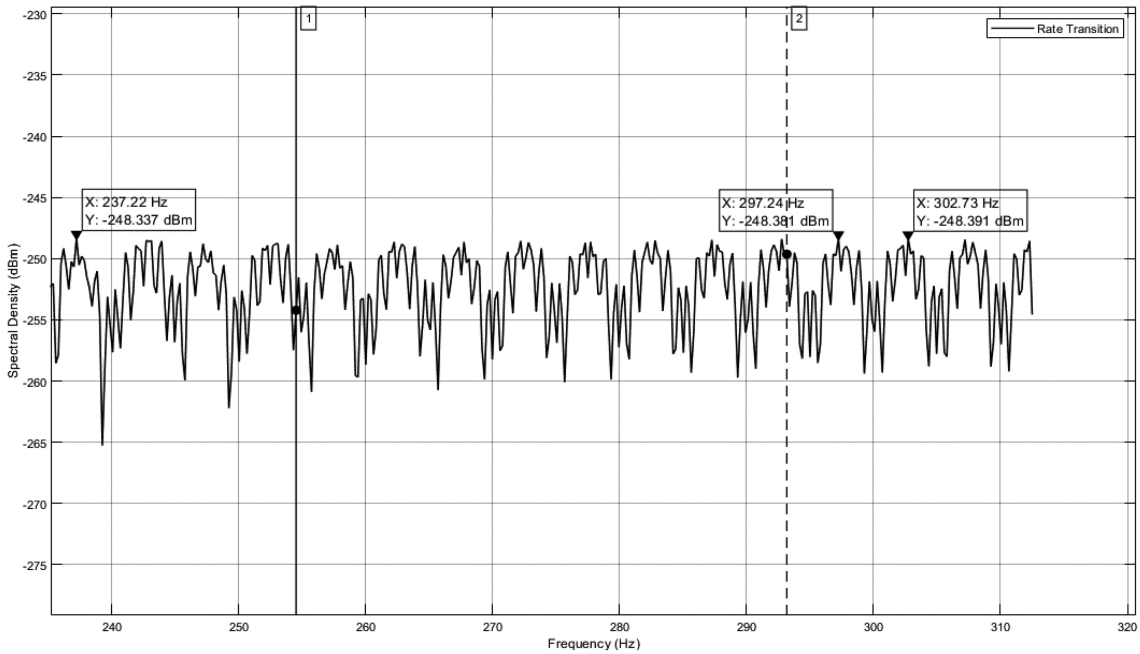

Fig. 10. Quasi perturbation state.

IV. CONCLUSIONS

Whereas the SG level control also provided complementary signal information from the sensors (S_1 and S_3) as the sensor load, the fluid flow sensors (S_2 and S_4) provided information and the control signal of the mass flow rate of the fluid (signal conditioner). The feedback signal provided the actuator signal to regulate the speed of the FW pump, based on the signal information from the SG level control, FW pump control, motor speed control, and valve actuator control. This study indicated the following:

1. The results from the analysis reveal considerable reduction of turbulence due to the introduction of drive signal and velocity vector as compensator.

2. The relative mass flow rate perturbation and pressure sensor provided relative pressure perturbation with constant Reynolds number, where the constant discharge coefficient of momentum of the deferential pressure depends on the critical velocity restriction of the valve.

3. The spectrum analyzer provided the plot of noise PSD (in dBm/Hz) that illustrated the peak as finder and distortion measurement, which provides the opportunity to reduce the impact of noise in order to improve the performance of the I&C system.

In this paper, the turbulent effect of water hammer in NSSS was analyzed. The introduction of modern digital control sensors provided information on the fluid flow rate entering the SG and the steam flow rate driving the steam turbine. The relative mass flow perturbation of the FW pump depends on the Reynolds number. The constant discharge coefficient as the momentum of the deferential pressure depends on the critical velocity restriction of the shutting and opening of the pressure relief valve. The average finite measurement of the total PSD (in dBm/Hz) over a specific period was measured using the Fourier transform. The programmable voltage driver responds to signals from the sensors to regulate the speed of the pump, which shows the potential of significantly reducing the impact of water hammer that could lead to a break and the resultant effect of LOCA.

Disclosure Statement

No potential conflict of interest was reported by the author(s).

ORCID

Frederick Agyemang http://orcid.org/0000-0003-2263-4269

References

1. D. TESTA and A. KUNKLE, "The Westinghouse Pressurized Water Reactor Nuclear Power Plant," Westinghouse Electric Corporation Water Reactor Divisions (1984).
2. B. ZHANG, W. WAN, and M. SHI, "Experimental and Numerical Simulation of Water Hammer in Gravitational Pipe Flow with Continuous Air Entrainment," *Water*, **10**, *7* (2018).
3. M. S. GHIDAOUI et al., "A Review of Water Hammer Theory and Practice," *Appl. Mech. Rev.*, **58**, *1*, 49 (2005); https://doi.org/10.1115/1.1828050.
4. A. SECK, "Numerical Solutions of Hyperbolic Systems of Conservation Laws Combining Unsteady Friction and Viscoelastic Pipes," *J. Hydroinf.*, **23**, *1*, 103 (2021); https://doi.org/10.2166/hydro.2020.119.
5. J. MARCINKIEWICZ, A. ADAMOWSKI, and M. LEWANDOWSKI, "Experimental Evaluation of Ability of Relap5, Drako®, Flowmaster2™ and Program Using Unsteady Wall Friction Model to Calculate Water Hammer Loadings on Pipelines," *Nucl. Eng. Des.*, **238**, *8*, 2084 (2008); https://doi.org/10.1016/j.nucengdes.2007.10.027.
6. A. S. TIJSSELING, "Water Hammer with Fluid–Structure Interaction in Thick-Walled Pipes," *Comput. Struct.*, **85**, *11–14*, 844 (2007); https://doi.org/10.1016/j.compstruc.2007.01.008.
7. E. YAO, G. KEMBER, and D. HANSEN, "Analysis of Water Hammer Attenuation in Applications with Varying Valve Closure Times," *J. Eng. Mech.*, **141**, *1* (2015); https://doi.org/10.1061/(ASCE)EM.1943-7889.0000825.
8. R. GODA et al., "Effects of Fluid Properties on Interfacial and Wall Friction Factors Under Counter-Current Flow Limitation in a Vertical Pipe with Sharp-Edged Lower End," *Nucl. Eng. Des.*, **373**, 111020 (2021); https://doi.org/10.1016/j.nucengdes.2020.111020.
9. F. DI MAIO et al., "A Multi-State Physics Modeling Approach for the Reliability Assessment of Nuclear Power Plants Piping Systems," *Ann. Nucl. Energy*, **80**, 151 (2015); https://doi.org/10.1016/j.anucene.2015.02.007.
10. Y. LIAO and D. LUCAS, "Possibilities and Limitations of CFD Simulation for Flashing Flow Scenarios in Nuclear Applications," *Energies*, **10**, *1*, 139 (2017); https://doi.org/10.3390/en10010139.

11. A. YAMANOUCHI, "Effect of Core Spray Cooling in Transient State after Loss of Coolant Accident," *J. Nucl. Sci. Technol.*, **5**, *11* (1968).
12. K. PETTERSSON et al., "Nuclear Fuel Behaviour in Loss-of-Coolant Accident (LOCA) Conditions" (2009) (unpublished).
13. I. F. BARNA, A. R. IMRE, and G. BARANYAI, "Theoretical and Experimental Study of Steam Condensation Induced Water Hammer Phenomena," *Proc. Int. Congress Advances in Nuclear Power Plants (ICAPP 08)*, Anaheim, California, June 8–12, 2008, American Nuclear Society.
14. I. F. BARNA et al., "Experimental and Theoretical Study of Steam Condensation Induced Water Hammer Phenomena," *Nucl. Eng. Des.*, **240**, *1*, 146 (2010); https://doi.org/10.1016/j.nucengdes.2009.09.027.
15. P. GRIFFITH, "Screening Reactor Steam/Water Piping Systems for Water Hammer," US Nuclear Regulatory Commission (1997).
16. I. FERENC BARNA and G. EZSÖL, "Multiple Condensation Induced Water Hammer Events, Experiments and Theoretical Investigations," *Kerntechnik*, **76**, *4* (2011).
17. I. F. BARNA et al., "Theoretical Study of Steam Condensation Induced Water Hammer Phenomena in Horizontal Pipelines," *Kerntechnik*, **80**, *5*, 420 (2015); https://doi.org/10.3139/124.110537.
18. R. D. BLEVINS, "Applied Fluid Dynamics Handbook," Van Nostrand Reinhold Company (1984).
19. "Application of Field Programmable Gate Arrays in Instrumentation and Control Systems of Nuclear Power Plants," International Atomic Energy Agency (2016).
20. C. H. YU, "Application of Persevel's Theorem on Evaluating Definite Integrals," *Turk. J. Anal. Number Theory* (2014).
21. R. N. BRACEWELL, *The Fourier Transform and Its Applications*, Vol. Mc-Graw-Hill, New York (1986).